Chemical and Process Engineering 2014, 35 (1), 19-33
DOI: 10.2478/cpe-2014-0002

SELECTION OF OPTICAL TOMOGRAPHY PARAMETERS FOR GAS BUBBLE SHAPE ANALYSIS

Mariusz R. Rząsa*

Technical University of Opole, Department of Thermal Engineering and Industrial Facilities,
ul. Mikołajczyka 5, 45-233 Opole, Poland

An optical tomograph in which a tested object is illuminated from five directions has been presented in the paper. The measurements of luminous intensity after changing into discrete signals (0 or 1) in the detectors equipped with 64 optical sensors were subjected to reconstruction by means of the matrix algorithm. Detailed description of the measuring sensor, as well as the principles of operation of the electronic system, has been given in the paper. Optical phenomena occurring at the phase boundary while transmitted through the sensor wall and phenomena inside the measuring space have also been taken into account. The method of the sensor calibration has been analysed and a way of technical solution of the problem under consideration has been discussed. The elaborated method has been tested using objects of the known shape and dimensions. It was found that reconstruction of the shapes of moving bubbles and determination of their main parameters is also possible with a reasonable accuracy.

Keywords: bubble shape, gas flow, optical tomography, two-phase measurement

1. INTRODUCTION

During two-phase gas-liquid flows through vertical and horizontal pipelines, various flow structures can occur, depending on streams of the delivered phases and physical and chemical properties of both phases (Magnaudet and Eames, 2000; Prosperetti, 2004). Assessment of the flow structure is often conducted by visual observation in a transparent channel (Leifer et al., 2003; Mayinger and Feldmann, 2001; Yonguk et al., 2005). It is not easy to include an observed flow to the given structure and such decisions are usually subjective, so averaging distribution of phase concentration at time and space is often accomplished by intuition. In this paper, the author proposes a method for evaluation of a gas-liquid flow using optical tomography. In measurements, shapes of moving bubbles are registered, then bubble dimensions are analysed and the parameters such as bubble motion velocity and its volume are determined. They can be used for estimation of volume fraction of gas and liquid. The presented solution allows to measure parameters of moving bubbles in the vertical direction (Figs. 1a, b). In vertical flows, distribution of gas phase concentration is usually symmetric. While the gas flows in horizontal direction, at small gas flows rates, bubble structures occur with greater bubble concentrations in the upper parts of the pipeline (Figs. 1c, d). In both horizontal and vertical pipes, the flows are characterised by highly variable dynamics of changes of instantaneous concentration distributions. Thus, image scanning should be performed at a very high rate. Only in stratified flows, the scanning rate is slightly lower.

*Corresponding author, e-mail: m.rzasa@po.opole.pl

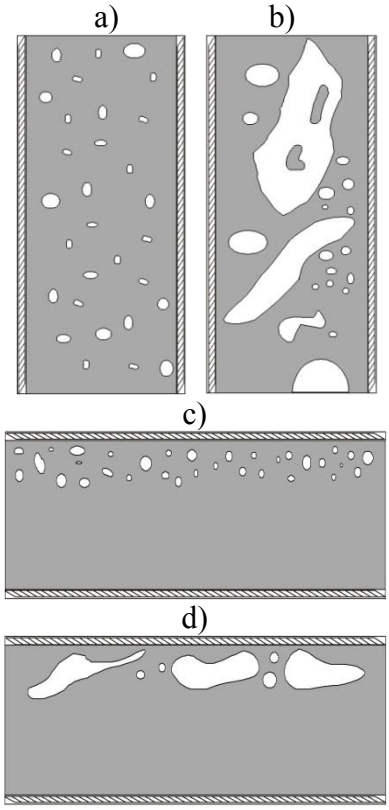

Fig. 1. Structures of gas-liquid flows reconstructed by the optical tomograph in:
a) vertical bubble flow, b) vertical churn flow, c) horizontal bubble flow, d) horizontal slug flow

2. OPTICAL TOMOGRAPHY – PRINCIPLE OF OPERATION

The main idea of optical tomography utilises optical phenomena occurring on the boundary between the phases. The measuring section is illuminated by a light beam, and next the intensity of light passing through the section in a chosen direction is measured (Fig. 2). The light emitted from the source passes through the tested section and is subject to partial absorption both in gas and liquid phases. Moreover, the light ray is reflected and scattered when passing through across a bubble. All these effects cause substantial light intensity attenuation on the way to the detector (Kawaguchi et al., 2002; Rząsa, 2009).

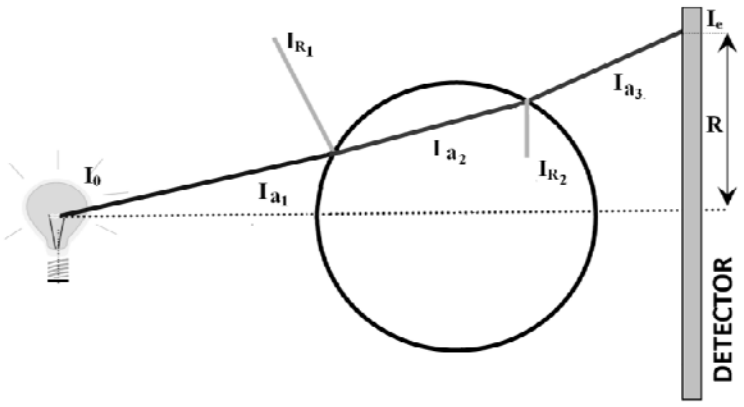

Fig. 2. Optical tomograph – principle of operation

Theoretical deliberations concerning phenomena occurring on the phase boundary were here limited to a single bubble. Consider a single light beam passing through the bubble. The ratio of the radiation intensity of light I_e detected on the sensor to that of the light emitted by the source I_0 was assumed as a

criterion for comparative purposes. Distribution of the light intensity field depends on the system geometry, and the bubble can be understood as a thin lens, where the light ray is subject to refraction, reflection and partial absorption. The ratio of the light intensity is expressed by the following general relationship Dugdale et al., 1993).

$$\frac{I_e}{I_0} = \delta r \, \delta b \;\; \delta a \tag{1}$$

The usage of this solution requires a transparency of pipeline`s walls in the measurement cross section. Also, it can be used for colored liquids, but the liquid must be transparent to a wavelength range of light.

2.1. Optical tomography

Illuminating the object with a dispersed beam of light is quite easy but the algorithm of reconstruction becomes much more complicated. The light is emitted from a five light source, and then it is detected in the field of the beam dissipation (Fig. 3).

The prototype tomography includes the pipeline 76 mm in diameter and five 55W light sources. The bulbs are located in 5 planes related to the pipeline axis (Fig. 3), so it is possible to determine velocities of moving objects. The distance between the successive layers is 7 mm. Five light detectors are connected opposite to the five light sources. A light detector consists of a matrix with 64 phototransistors. The phototransistors are set up inside collimations tube (Rząsa and Pląskowski, 2003).

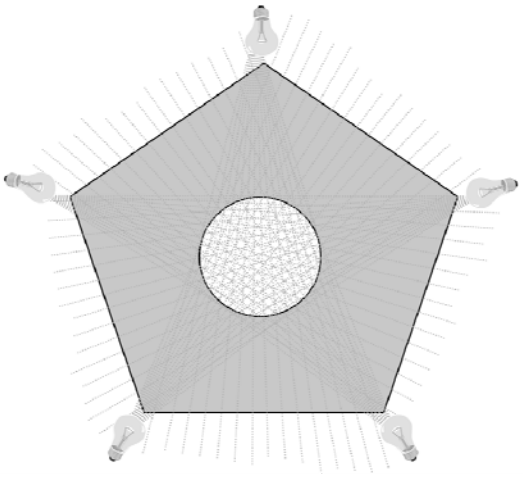

Fig. 3. The measuring sensor

In systems with a dispersed light beam, the light beams are usually distributed along the pipeline, so it is possible to measure the velocity of moving bubbles. For example, for the version including five projections, all the light beams were distributed at the same distance. However, it is possible to displace only some selected beams, and the remaining ones are placed in one plane.

2.2. Reconstruction algorithm

In a homogeneous medium, light propagates along the straight paths, and under such conditions image reconstruction is not very complicated. The relation between a discrete measuring value Φ_M and the reconstruction function *f(x,y)* is expressed by the following linear relationship (Kihm et al., 1998; Reinecke and Mewes, 1996; Tarvainen et al., 2008):

$$\Phi_M = \int_s f(x,y)ds \tag{2}$$

For a given light ray, the signal path through the measuring space from the transmitter to the receiver does not depend on the values in the fields of reconstruction function *f(x,y)* which are not crossed by the ray. The function of the measured values Φ_M depends only on the function of distribution *f(x,y)* along the given path *s* Thus, the efficient algorithm is based on the matrix method. In this method, the matrix of the values representing the object state registered by suitable measuring sensors is a base of reconstruction. The values of the function elements in suitable nodes are determined from the data coming from object illumination by the streams passing at different angles (Cao et al., 2007; Dehghani et al., 2009). Reconstruction consists in solving the linear matrix equation:

$$W \times F = P \tag{3}$$

where

$$W = \begin{bmatrix} w_{11} & w_{12} & \cdots & w_{1m} \\ w_{21} & w_{22} & \cdots & w_{2m} \\ \vdots & \vdots & \cdots & \vdots \\ w_{n1} & w_{n2} & \cdots & w_{nm} \end{bmatrix} \quad F = \begin{bmatrix} f_1 \\ f_2 \\ \vdots \\ f_n \end{bmatrix} \quad P = \begin{bmatrix} \Phi_1 \\ \Phi_2 \\ \vdots \\ \Phi_m \end{bmatrix} \tag{4}$$

The matrix *W* is a sensitivity map (Cao et al., 2007) and is individual for each sensor. From the above equation we obtain *n* linear equations, a solution of which is the matrix of function values of the object image. This method is applicable for reconstruction of images of large contrast.

In the case of reconstruction from a discrete tomography, when the measuring data are `0` or `1`, a certain modification of the matrix method was introduced. It consists in direct calculation of the image function with no necessity of solving the system of equations. The matrix equation takes the form:

$$F[n] = W[n,m] \times \Phi[m] \tag{5}$$

After reconstruction, the image can be subjected to Image Processing in order to improve quality of reconstruction. Thresholding is one of the methods of image quality improvement. In this method, only two values ‘1’ or ‘0’ are assigned to image function elements f_i according to the algorithm:

$$f_i = \begin{cases} 1 & for \quad f_i \geq a_p \\ 0 & for \quad f_i < a_p \end{cases} \tag{6}$$

Another method of image correction is to improve contrast by gaining the fields of high values and attenuation of the fields of low values. For normalised values (all the field values are included in the interval from 0 to 1), the contrast function takes the form:

$$f_i' = (f_i)^K \tag{7}$$

where *K* is a coefficient of contrast. In many cases it is proper to apply both methods with suitable coefficients. In numerous cases it is advisable to apply both methods simultaneously with appropriately selected coefficients.

2.3. Determination of Sensitivity Charts

When determining sensitivity charts we must take into account the structure of the measuring sensor and phenomena occurring inside the sensor. The sensor shown in Fig. 3 was applied for the tests. The

measuring space was inside a glass tube 1, D = 76 mm in inside diameter and h = 1.7 mm in thickness. The pipe was placed inside a pentagon 2 made of glass. The sides of the pentagon were shaped along the arc of the radius R = 300 mm, corresponding to the natural angle of propagation of the light beam. The pentagonal boxing was filled by the same liquid that was in the measuring space, so the same coefficients of light refraction could be kept in all the space of light ray propagation. Also the detectors had a suitable curvature, fitted to the boxing curvature. Thus, light refraction did not occur at the light passage between the tomography boxing and the detector. The inlet of the light ray had a shape of an arc of radius r = 30 mm.

Measurements are performed with detectors receiving the light beam after passage through the tested space (64 detectors for each of five planes). If the ray path between the source and the detector is known, we are able to reconstruct the image under a suitable sensitivity matrix.

The glass tube can be simulated as an area of the space with a certain refraction coefficient, limited by two cylinders. Since all the detectors are in one plane and they are the same, the calculations can be performed for one plane, and then the chart should be turned by a suitable angle. Geometry of the light ray passing through the measuring sensor for one plane is shown in Fig. 4.

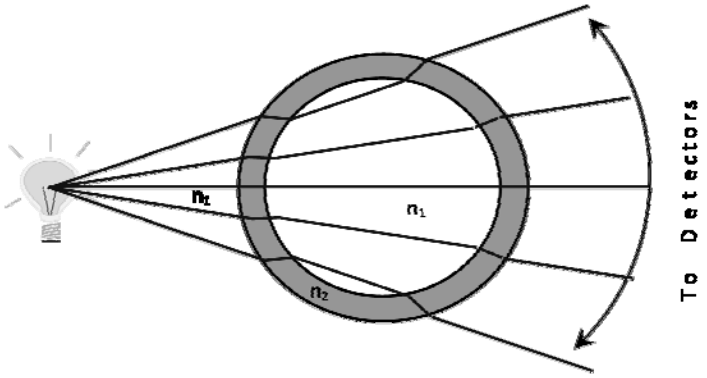

Fig. 4. Geometry of the light ray in the measuring space (Rząsa, 2009)

In order to determine the sensitivity matrix we should observe the ray path. After its release from the source, it is subject to refraction at the boundary between two media n_1 and glass n_2 according to the Snell law. Next, the ray is subject to three successive refractions (the space filled with homogeneous medium) - Fig. 4. Outside the tube, the ray reaches the sensor at an angle different from that at which it was sent. Since it is difficult to calculate the ray path with the use of an algebraic method, iterative methods have been applied. The rays coming from the source are calculated with the applied steps. Thus, the searched ray can be calculated with any finite accuracy.

The sensitivity matrix has been determined assuming that values of particular fields of the matrix are proportional to the ratio of the area covered by the ray of the light beam to the field area of the sensitivity matrix.

2.4. Light Beam Tracking Method

Light beams are emitted from the source to the detector at various angles. Passageways of particular beams are then a base for determining volumes of particular areas of sensitivity map. It is assumed that the volume sensitivity map area alleys equal to 1 when the light beam goes through a given area (Fig. 5).

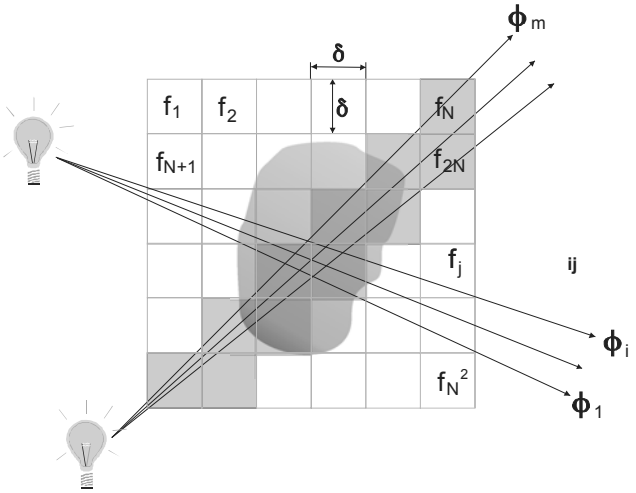

Fig. 5. The idea of sensitivity map determination

$$W[i,j] = \begin{cases} \dfrac{1}{k} & for \quad k \geq 2 \\ 0 & for \quad k < 2 \end{cases} \tag{8}$$

where k is a number of light beams going through j-th area of image function.

This method is based on an assumption that the values of particular areas of sensitivity maps are proportional to the light beam covered area to the total of the areas of the image field.

The idea of determination of the matrix W is shown in Fig. 6. Particular elements of the matrix W are suitable fractions proportional to the area of the field j illuminated by the radius i. The sensitivity matrix W is calculated from:

$$W[i,j] = \begin{cases} \dfrac{A_{ij}}{\sum_{i=1}^{m} A_{ij}} & for \quad k \geq 2 \\ 0 & for \quad k < 2 \end{cases} \tag{9}$$

where k is a number of radii passing through the j-th field of the image function, and A_{ij} is area covered by the beam Φ_i in the image field f_j.

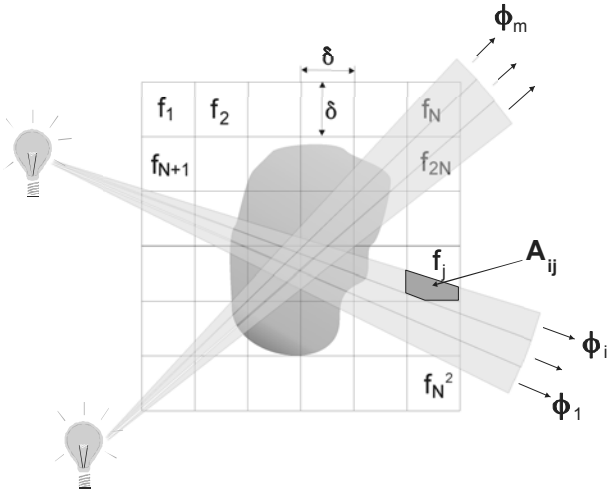

Fig. 6. The idea of matrix W determination (Rząsa, 2009)

2.5. Light beam limited area tracking method at a constant field

This method is based on an assumption that the volumes of particular areas of the sensitivity maps are proportional to the relation between the light beam covered area and the total of the areas that constitute the common part. The way of scanning is identical with the former one (Fig. 6) whereas the way of determining particular areas has been changed. An exemplary scanning of one area by four light beams coming from four different directions is shown in Fig. 7.

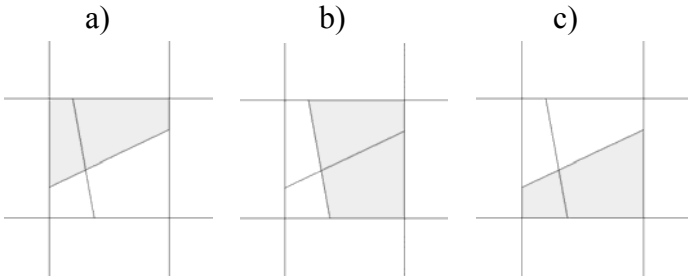

Fig. 7. Sample scanning of one area for four light beams

It is noticeable that the beam in Fig. (7a) has common parts with Fig. (7b) and (7c). This results in forming additional areas being a total of areas of particular beam pairs (Fig. 8).

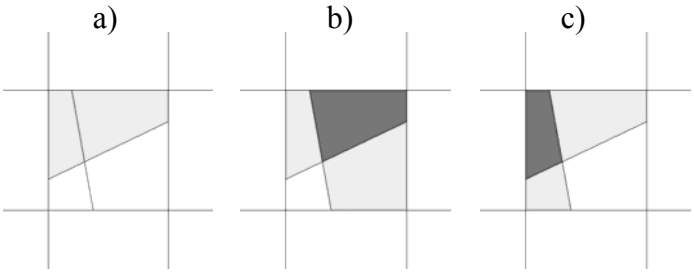

Fig. 8. Areas including common part of several beams

$$W[i,j]=\begin{cases}\dfrac{A_{ij}}{\sum_{i=1}^{m} C_{ij}} & for \quad k \geq 2 \\ 0 \quad for \quad k < 2\end{cases} \tag{10}$$

where k is a number of beams going through j-th image function, and C_{ij} is area covered by a beam Φ_i in the image field f_j.

2.6. Tests of Sensitivity Maps

The tests carried out on the correctness of the algorithm of the image reconstruction are presented in this section. The tests aimed at reconstructing the images of two moving bubbles for three different sensitivity maps.

An example of how the methods function is shown in Fig. 9. Figure 9a presents image reconstruction with use the sensitivity map generated with the light beam tracing method. Artefacts which will lead to considerable errors in the case of determining the volume fraction are clearly visible. In fact such an image is practically useless for further calculations. Application of thresholding considerably improves reconstruction results (Fig. 9b), although it does not completely eliminate artefacts. Besides, it causes

vanishing of some areas which ought to be marked as gas. Figure 9c shows the results for contrast upgrading application. Such a solution much better reflects oval shapes of the bubbles but the artefacts are still visible. This method, however, does not result in setting a clear boundary between phases as apposed to thresholding. Simultaneous application of image upgrading and thresholding (Fig. 9d) enables setting apart a clear phase boundary at the proper assignment appropriate areas to the gas and the liquid. The artefacts that still do appear considerably reduce the application range of the above method in determining sensitivity maps. In real measuring systems it is possible that a value of function fi does not reach 1 or 0. It is caused by disturbances of measurements and, in a consequence, errors. In such a case, we can use the function values according to:

$$f_i = \begin{cases} 1 & for \quad f_i \geq a_p \\ 0 & for \quad f_i < a_p \end{cases} \tag{11}$$

A different solution of reduced artefacts is possible of uses the contrast function. For the normalised image function elements the contrast function is calculated:

$$f_j^{'} = \left(f_j\right)^{a_n} \tag{12}$$

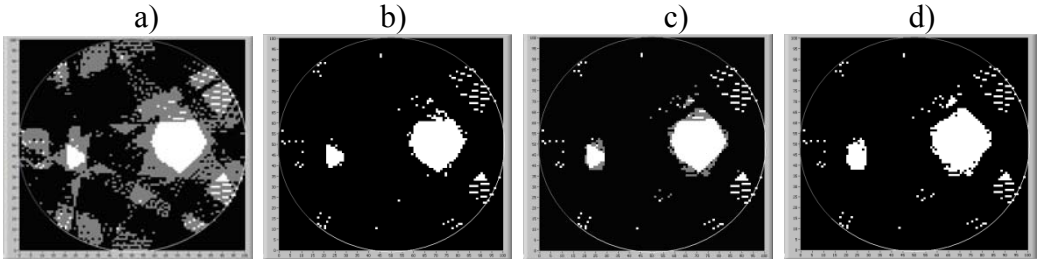

Fig. 9. Sample image obtained with the use of an optical tomograph for a sensitivity map with the light beam tracing method: a) image reconstruction, b) with application of thresholding $a_p = 0.8$, c) with application of contrast upgrading $a_n = 3$, d) with simultaneous application of contrast upgrading and thresholding $a_p = 0.8$ and $a_n = 3$

Figure 10 show the results of reconstruction with the use of the sensitivity map based on tracing an area limited by a Light beam.

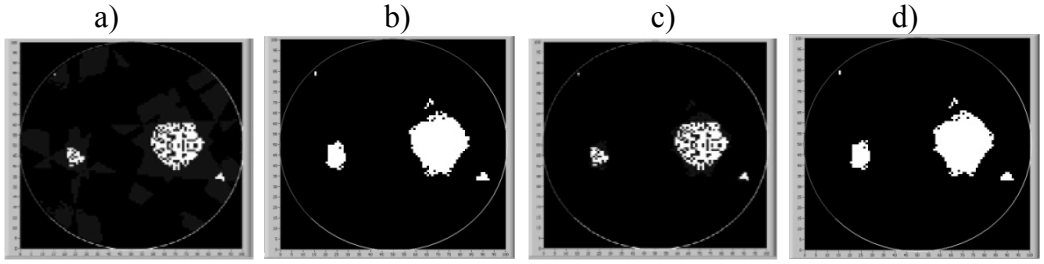

Fig. 10. Sample image obtained with the use of an optical tomograph for a sensitivity map with the light beam limited area tracing method a) image reconstruction, b) with an application of thresholding $a_p = 0.8$, c) with an application of contrast upgrading $a_n = 3$, d) with a simultaneous application of contrast upgrading and thresholding $a_p = 0.5$ and $a_n = 3$

As compared to the image in Fig. 9, the presence of the artifacts is also noticeable. Furthermore, considerably fewer areas have values that explicitly would qualify them as gas or as liquid. However, application of thresholding considerably improves the results of reconstruction (Fig. 10b). In this particular image the artifacts were corrected to a large extent. Such a solution should be recommended

to a wide usage in determining flow parameters. Contrast upgrading (Fig. 10c) leads to similar results although it still does not improve the phase boundary clarity. An application of both the contrast upgrading and the thresholding simultaneously does not actually improve the image quality as compared to the thresholding alone (Fig. 11d). This may lead to a conclusion that there is no justification for the image upgrading method for a sensitivity map based on tracing the light beam limited area.

The results of reconstruction for the sensitivity map generated with the light beam limited area at a constant field method are shown in Figure 11. The image basically does not contain gas assigned areas but clearly visible are the smaller number artifacts as compared to the former solutions. Figure 11b presents the results of reconstruction with the use of thresholding; in this case the boundary between phases with a small number of appearing artifacts is clear. When compared to Figure 10b this image is slightly worse with respect to the artifacts but it better reflects oval shapes of the bubbles. Similar results can be obtained whit the use of contrast upgrading. Host artifacts disappear whereas it is only an area of the field value from a value interval f_j= 0.33-0.66 (Fig. 11c). The application of thresholding and contrast upgrading simultaneously leads to formation of a clear boundary between the phases (Fig. 11c). This image is comparable with that in Fig. 12d. Similarly, only sparse artifacts are visible here, although they lay out differently in the image area. On such a basis we can expect similar results in determining the flow parameters.

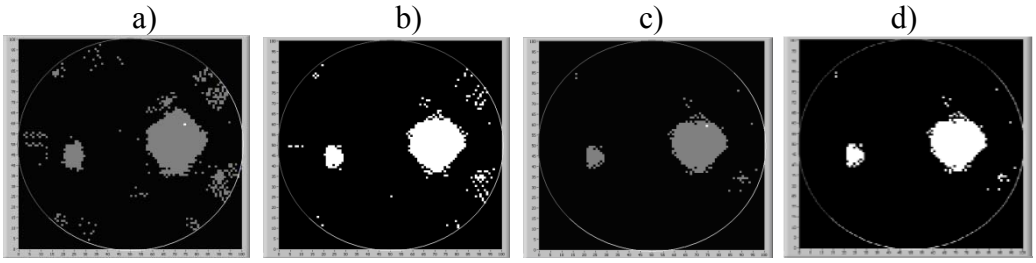

Fig. 11. Sample image obtained with the use of an optical tomograph for a sensitivity map with the light beam tracing method a) image reconstruction, b) with an application of thresholding a_p = 0.8, c) with an application of contrast upgrading a_n = 3, d) with a simultaneous application of contrast upgrading and thresholding a_p = 0.8 and a_n = 3

3. DETERMINING OF BUBBLE VELOCITY

As a consequence of displacement of the light beams in the longitudinal direction of the pipeline, it is possible to determine only the velocity component in this direction. However, this parameter is very important because it can be used for determination of the third dimension of the moving objects, necessary for their volume determination. If two detectors are parallel, velocity determination of the moving object consists in the time analysis of signals received from the detectors. Typical signal courses from two detectors are shown in Fig. 12.

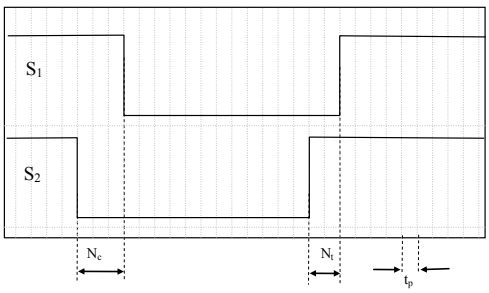

Fig. 12. Typical time courses from two detectors

On the registered courses we can observe time displacement (N_c and N_t) connected with the bubble movement between the detectors. This is the time necessary for the bubble to cover a distance between two layers of the sensors. Time measurement is connected with an error, so suitable times (N_c, N_t) are equal or not. In this case, the correlation methods should be used for determination of the velocity. The mean velocity is determined from the mean time of displacement between the courses.

$$w_s = \frac{s}{n_Z t_p} \tag{13}$$

A number of the clock strokes n_Z was determined with the correlation method by determination of the number n for which the correlation function reaches its maximum value.

$$K_{\max\limits_{n_Z \to N_p}} = \sum_{i=0}^{N_p - n_Z} d_i^1 d_{i+n_Z}^2 \tag{14}$$

In practice, it is not necessary to analyse correlation in all the time intervals of the signal. It is enough to limit N_p to the given maximum real number of samples which could occur for the given flow rate. This number results from the maximum possible velocity of the air bubbles moving in the considered flow.

In the case of the dissipated beam (Fig. 4), this seems to be much more difficult since the detectors determining the velocity N_c are placed in one plane being displaced at a certain angle. In such a case, determination of displacement between particular bubbles is important because of definition of the longitudinal velocity and displacement of time sequences. In order to displace the measured signals, the method using the correlation function was applied (Beck and Pląskowski, 1987). If a delay of the signal between particular measuring places is known, it is possible to transfer the signal in time.

The flow velocity can be determined when the distances between all combinations of the measuring planes are known. This problem is rather complex because in this case the delay matrix is present, but not the displacement number (Rząsa and Pląskowski, 2003). For example, for the sensor with five detectors the matrix takes the following form:

$$N^{shift} = \begin{bmatrix} 0 & n_{1,2} & n_{1,3} & n_{1,4} & n_{1,5} \\ n_{2,1} & 0 & n_{2,3} & n_{2,4} & n_{2,5} \\ n_{3,1} & n_{3,2} & 0 & n_{3,4} & n_{3,5} \\ n_{4,1} & n_{4,2} & n_{4,3} & 0 & n_{4,5} \\ n_{5,1} & n_{5,2} & n_{5,3} & n_{5,4} & 0 \end{bmatrix} \tag{15}$$

The displacement chart can be used for determination of the velocity matrix. The gas and the liquid can flow in the same direction or they can flow in inverse directions. The mean bubbles velocity is determined from:

$$w_s = \frac{1}{(N-1)^2} \sum_{i=1}^{N-1} \sum_{j=1}^{N-1} w_{i,j} \tag{16}$$

The test stand shown in Figure 13 was build in order to verify the algorithm for determination of the velocity. The optical tomograph includes five illuminating planes; the distances between them are identical. Such a solution allows to determine the velocity of the moving bubbles. In order to determine dynamical properties of the optical tomography, a motor with a transmission gear was placed above the measuring sensor. The transmission allows changing rotations of the wheel. A line with a weight is wound on the wheel. The weight passes through the measuring space of the tomography scanner and simulates the bubble motion. Constant rotations of the motor provide uniform motion in vertical direction. A series of measurements was performed in order to estimate an error in the velocity of bubbles moving along the pipeline axis.

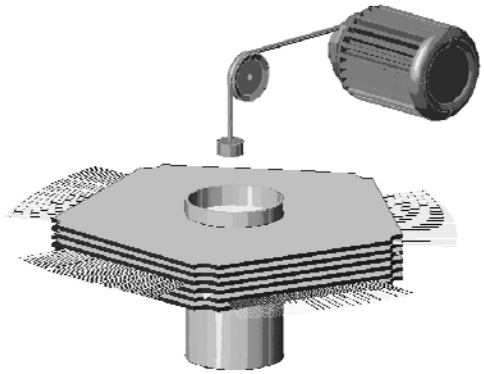

Fig. 13. The stand for tests of dynamical properties of the optical tomograph

Sample results of verification of the algorithm for signal correlation and displacement of particular planes are shown in Fig. 14 (Rząsa et al, 2007). The presented results come from the test where the object moving with a constant velocity v = 0.05 m/s, moved within the measuring sensor. Figure 14a shows signal courses coming from five detectors of the optical sensor. Mutual displacements of signals caused by displacement of the object in the longitudinal direction can be easily found from that figure. In order to correct the reconstruction it is necessary to bring the courses to one plane. The results of the algorithm for signal correlation are shown in Fig. 14b.

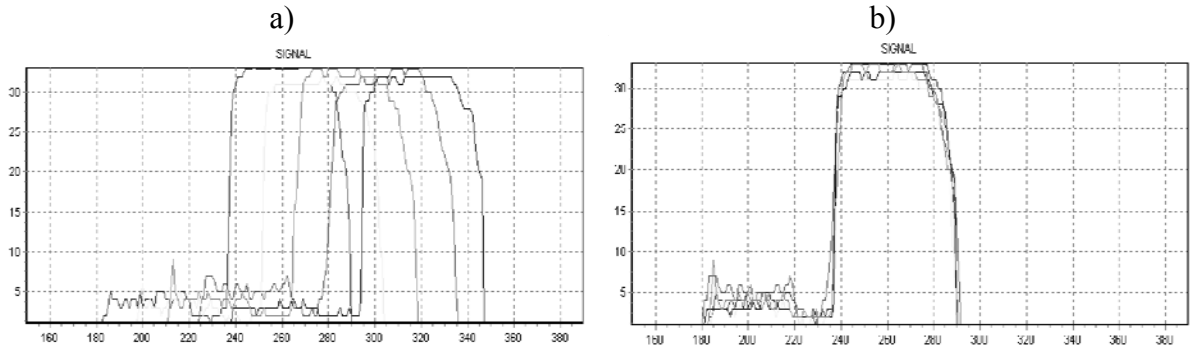

Fig. 14. Time courses of the data from measurements from five sensors a) before correlation, b) after correlation

3.1. Tests Results

Some tests were performed in order to evaluate quality of image reconstruction, namely an object of the known shape and dimensions was displaced inside the optical tomograph (Fig. 15a). A three-dimensional image of the object was reconstructed in order to evaluate correctness of the algorithm moving particular signals from the detectors.

The results of this reconstruction are shown in Fig. 15b. The cylindrical part was reconstructed very well. Reconstruction of the hook is worse; it is caused by small diameter of the bar (2 mm), being at the threshold of the assumed resolution of the tomograph.

To estimate the volume fraction it is necessary to determine the mean volume of gas transported together with the liquid. From the tomography we can obtain images of the cross section at a constant time step. It is a basis for determination of volume of the gas flowing through the chosen measuring section. Since the image formed by the optical tomography includes a regular network and each successive frame is registered at a constant time step, so it is possible to calculate gas volume in a way shown in Figure 16. Particular image fields are of the same shapes and volumes.

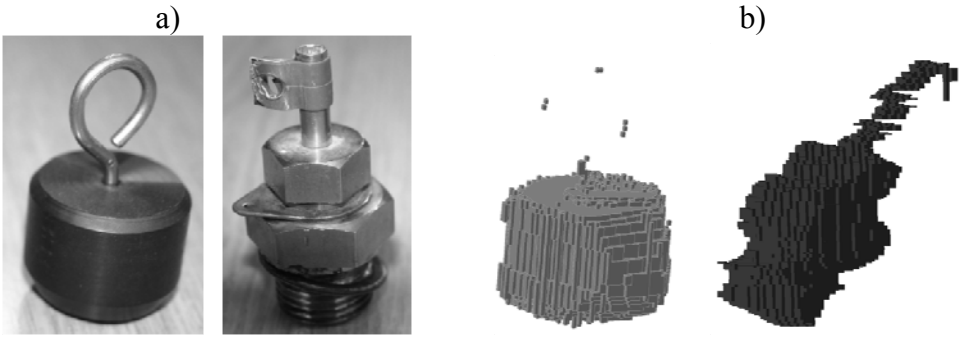

Fig. 15. Reconstruction of the tested object: a) objects, b) image after reconstruction

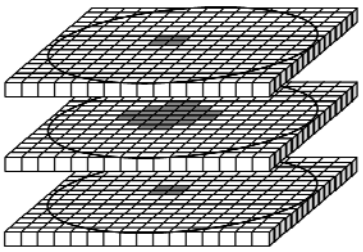

Fig. 16. Idea of gas volume determination based on the image from the 3D tomography

Thus, volume estimation consists in determination of a number of the fields covered with gas and multiplication of this quantity by a unit volume.

$$V_g = n_g V_j = n_g \left(\frac{D}{R} \right)^2 d_z \tag{17}$$

Determination of the distance d_z is based on the gas motion velocity. Since the time of the distance between the successive images from the tomography is known and remains constant, the distance d_z is calculated from:

$$d_z = w_S \cdot t_p \tag{18}$$

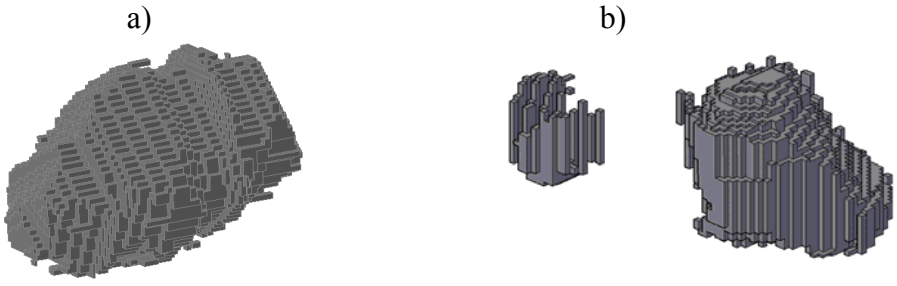

Fig. 17. The results of reconstruction: a) single bubble, b) group of bubbles

For example, for the bubble measured with the optical tomography and shown in Fig. 17a, for which the sampling time is t_p = 10 ms, image resolution N = 100, sensor diameter D = 76 mm, bubble motion velocity amounts w_s = 0.045 m/s. The bubble contains n_g = 54183 elements.

Thus, the determined volume is V_g = 0.000014 m^3 = 14 ml. The results of reconstruction of group of moving bubbles in vertical flow are shown in Fig. 17b. The bubbles have different shapes and volumes.

This solution enables to study the mechanism of gas bubble formation. The measurements of bubble shape creation as well as bubble volume provide important parameters for verification of theoretical models. Figure 18 shows sample images of bubbles generated at the outlet of a nozzle (d = 2 mm). The results are presented for different gas streams.

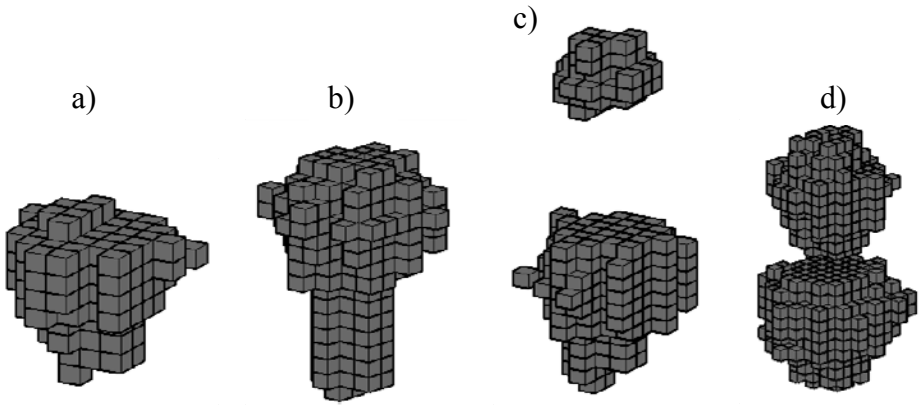

Fig. 18. Bubble shapes of gas streams: a) 0.1 cm^3/s, b) 0.6 cm^3/s, c) 1 cm^3/s, d) 4 cm^3/s

6. CONCLUSIONS

The presented method based on optical tomography allows to measure even very small objects placed in the measuring space. It is possible to reconstruct the shapes of the moving bubbles and calculate their main parameters. Application of discrete signal processing simplifies structure of the tomography, calibration of the sensor and reconstruction algorithm, respectively. This is very important in the systems where fast recording of data is required. The prototype tomograph allows to record up to 1000 frames per second. The proposed solution consisting of 5 projections seems to be optimal and an increase of the number of detectors seems to be useless. The proposed solution is applicable when investigating the shape and determining the volume fraction for selected structures occurring in the gas-liquid two phase flow.

SYMBOLS

a_n	contrast coefficient
a_p	threshold coefficient
D	internal diameter of the tomograph, m
d^1, d^2	data of the signals S_1 and S_2
d_z	height of the slice, m
$f(x,y$	reconstruction function
f_j	element of reconstruction function
I_e	intensity of light falling on the sensor, lx
I_0	intensity of light emitted by the source, lx
m	number of measuring sensors
N	number of detectors
N_p	total number of samples
N_c, N_t	time displacement, s
n	number of image function fields
n_g	number of the image pixels covered with

n_z average number of samples
R resolution of the image from the tomograph
s distance between the detectors level, m
t_p sampling time, s
V_j unit volume, m^3
$w_{i,j}$ velocity determined from correlation of signals between the detectors i and j, m/s
w_s bubble velocity, m/s

Greek symbols

α angle, deg
δb coefficient of intensity loss caused by light dissipation
δa coefficient of intensity loss caused by light absorption
δr coefficient of intensity loss caused by light reflection,
Φ_M discrete measuring value

REFERENCES

Beck M.S. and Pląskowski A., 1987. *Cross correlation flowmeters–their design and application*. Ed. Adam Hilger, Bristol, UK.

Cao N, Nehorai A, Jacobs M., 2007. Image reconstruction for diffuse optical tomography using sparsity regularization and expectation-maximization algorithm. *Opt. Express*, 15, 13695–13708. DOI: 10.1364/OE.15.013695.

Dehghani H., Srinivasan S., Pogue B.W, Gibson A., 2009. Numerical modelling and image reconstruction in diffuse optical tomography. *Philos. Trans. R. Soc. London, Ser. A*, 367, 3073–3093. DOI: 10.1098/rsta.2009.0090.

Dugdale P., Green R. G., Hartley A. J., Jackson R. G., and Landauro J., 1993. Characterisation of single bubbles by an optical tomographic system. *Conference of Workshop on Proces Tomography, Karlsruhe*.

Kawaguchi T., Akasaka Y., Maeda M., 2002. Size measurements of droplets and bubbles by advanced interferometric laser imaging technique. *Meas. Sci. Technol*., 13, 308–315. DOI: 10.1088/0957-0233/13/3/312.

Kihm K.D., Ko H.S., Lyons D.P., 1998. Tomographic identification of gas bubbles in two-phase flows with the combined use of the algebraic reconstruction technique and the genetic algorithm. *Opt. Lett.*, 23, 658–660. DOI: 10.1364/OL.23.000658.

Leifer I., de Leeuw G., Cohen L.H., 2003. Optical measurement of bubbles: system design and application. J. *Atmos. Oceanic Technol.*, 20, no. 9, 1317–1332. DOI: 10.1175/1520-0426(2003)020<1317:OMOBSD>2.0.CO;2

Magnaudet, J., Eames, I., 2000. The motion of high-Reynolds-number bubbles in inhomo-geneous flows. *Annu. Rev. Fluid Mech*., 32, 659–708. DOI: 10.1146/annurev.fluid.32.1.659.

Mayinger F., Feldmann O., 2001. *Optical measurements - Techniques and applications*. 2nd Edition, Heidelberg, Springer.

Prosperetti, A., 2004. Bubbles. *Phys. Fluids*, 16, 1852–1865. DOI: 10.1063/1.1695308.

Reinecke N., and Mewes D., 1996. Recent developments and industrial/research applications capacitance tomography. *Meas. Sci. Technol*., 7, 233–246. DOI: 10.1088/0957-0233/7/3/004.

Rząsa M.R., 2009. The measuring method for tests of horizontal two-phase gas–liquid flows, using optical and capacitance tomography. *Nucl. Eng. Des.*, 239, 699–707. DOI: 10.1016/j.nucengdes.2008.12.020.

Rząsa M.R., Grudzien K., Przywarski R., Romanowski A., Wajman R., 2007. The discrete optical tomograph including five projections. *5th World Congress on Industrial Process Tomography*, Bergen, Norway, 3-6 September 2007.

Rząsa M.R., Pląskowski A., 2003. Application of optical tomography for measurements of aeration parameters in large water tanks. *Meas. Sci. Technol*., 14, 199–204. DOI: 10.1088/0957-0233/14/2/307.

Tarvainen T., Vauhkonen M., Arridge S.R., 2008. Gauss–Newton reconstruction method for optical tomography using the finite element solution of the radiative transfer equation. *J. Quant. Spectrosc. Radiat. Transfer*, 109, 2767–2778. DOI: 10.1016/j.jqsrt.2008.08.006.

Yonguk R., Kuang-An C., Ho-Joon L., 2005. Use of bubble image velocimetry for measurement of plunging wave impinging on structure and associated greenwater. *Meas. Sci. Technol*., 16, 1945–1953. DOI: 10.1088/0957-0233/16/10/009.

Received 06 December 2012
Received in revised form 20 November 2013
Accepted 10 December 2013